FTIR Spectroscopy of the O Photointermediate in *pharaonis* Phoborhodopsin†

Yuji Furutani,‡,§,|| Masayuki Iwamoto,⊥ Kazumi Shimono,⊥ Akimori Wada,# Masayoshi Ito,# Naoki Kamo,⊥ and Hideki Kandori*,‡,||

Department of Materials Science and Engineering, Nagoya Institute of Technology, Showa-ku, Nagoya 466-8555, Japan, Department of Biophysics, Graduate School of Science, Kyoto University, Sakyo-ku, Kyoto 606-8502, Japan, Laboratory of Biophysical Chemistry, Graduate School of Pharmaceutical Sciences, Hokkaido University, Sapporo 060-0812, Japan, Graduate School of Organic Chemistry for Life Science, Kobe Pharmaceutical University, Higashinada-ku, Kobe 658-8558, Japan, and Technology (CREST), Japan Science and Technology Corporation, Kyoto 606-8502, Japan

Received December 24, 2003; Revised Manuscript Received February 17, 2004

ABSTRACT: *pharaonis* phoborhodopsin (*p*pR; also called *pharaonis* sensory rhodopsin II, *p*sR-II) is a photoreceptor protein for negative phototaxis in *Natronobacterium pharaonis*. During the photocycle of *p*pR, the retinal chromophore is thermally isomerized from the 13-cis to all-trans form. We employed FTIR spectroscopy of *p*pR at 260 K and pH 5 to reveal that this isomerization occurs upon formation of the O intermediate (ppR$_O$) by using *p*pR samples reconstituted with 12,14-D_2-labeled retinal. In ppR$_O$, C═O stretching vibrations of protonated carboxylates newly appear at 1757 (+)/1722 (−) cm^{-1} in H_2O and at 1747 (+)/1718 (−) cm^{-1} in D_2O in addition to the 1765 (+) cm^{-1} band of Asp75. Amide I vibrations are basically similar between ppR$_M$ and ppR$_O$, whereas unique bands of ppR$_O$ are also observed such as the negative 1656 cm^{-1} band in D_2O and intense bands at 1686 (−)/1674 (+) cm^{-1}. In addition, O−D stretching vibrations of water molecules in the entire mid-infrared region are assigned for ppR$_M$ and ppR$_O$, the latter being unique for *p*pR, since it can be detected at low temperature (260 K). The ppR$_M$ minus *p*pR difference spectra lack the lowest frequency water band (2215 cm^{-1}) observed in the ppR$_K$ minus *p*pR spectra, which is probably associated with water that interacts with the negative charges in the Schiff base region. It is likely that the proton transfer from the Schiff base to Asp75 in ppR$_M$ can be explained by a hydration switch of a water from Asp75 to Asp201, as was proposed for the light-driven proton-pump bacteriorhodopsin (hydration switch model) [Tanimoto, T., Furutani, Y., and Kandori, H. (2003) *Biochemistry 42,* 2300−2306]. In the transition from ppR$_M$ to ppR$_O$, a hydrogen-bonding alteration takes place for another water molecule that forms a strong hydrogen bond.

pharaonis phoborhodopsin (*p*pR)[1] from *Natronobacterium pharaonis* is a member of the archaeal rhodopsin family [bacteriorhodopsin, halorhodopsin, sensory rhodopsin (also called sensory rhodopsin I), phoborhodopsin (also called sensory rhodopsin II)] (*1*, *2*). *p*pR is a photosensor for negative phototaxis which activates the cognate transducer protein, *p*HtrII, upon light absorption. It possesses a retinal chromophore which is connected to one of its seven transmembrane helices, similarly to the case of well-studied proton-pump bacteriorhodopsin (BR) (*1*−*4*). In *p*pR and BR, the retinal forms a Schiff base linkage with Lys205 or Lys216, respectively, and the protonated Schiff base is stabilized by a negatively charged counterion, Asp75 or Asp85, respectively. Light absorption by *p*pR triggers trans-cis photoisomerization of the retinal chromophore in its electronically excited state (*5*), followed by rapid formation of the ground-state species such as the K intermediate (*6*). The same process occurs in BR. Relaxation of the primary intermediates leads to the formation of late intermediates, such as ppR$_L$, ppR$_M$, ppR$_N$, and ppR$_O$. The structural changes of protein in these intermediates eventually lead to the activation of *p*HtrII.

We started a comparative investigation of structural changes in *p*pR and BR by means of low-temperature FTIR spectroscopy. The results on the primary K intermediate revealed the structural similarity between *p*pR and BR in the polyene chain of the chromophore (*7*), hydrogen bonds of internal water molecules (*8*), and protonated retinal Schiff base (*9*). These observations were consistent with the similar crystallographic structures of *p*pR (*10*, *11*) and BR (*12*, *13*). In contrast, the structural alteration in the K state after photoisomerization was more extended in *p*pR than in BR (*7*). Such observation was also reported by X-ray crystal-

† This work was supported in part by grants from the Japanese Ministry of Education, Culture, Sports, Science, and Technology to H.K. and by research fellowships from the Japan Society for the Promotion of Science for Young Scientists to Y.F., M.I., and K.S.

* To whom correspondence should be addressed. Phone/Fax: 81-52-735-5207. E-mail: kandori@nitech.ac.jp.

‡ Nagoya Institute of Technology.

§ Kyoto University.

|| CREST.

⊥ Hokkaido University.

Kobe Pharmaceutical University.

[1] Abbreviations: *p*pR, *pharaonis* phoborhodopsin; ppR$_K$, K-intermediate of *p*pR; ppR$_L$, L-intermediate of *p*pR; ppR$_M$, M-intermediate of *p*pR; ppR$_N$, N-intermediate of *p*pR; ppR$_O$, O-intermediate of *p*pR; *p*HtrII, *pharaonis* halobacterial transducer II; BR, light-adapted bacteriorhodopsin that has all-*trans*-retinal as its chromophore; HOOP, hydrogen-out-of-plane vibration; DM, *n*-dodecyl β-D-maltoside; PC, L-α-phosphatidylcholine.

10.1021/bi036316b CCC: $27.50
Published on Web 04/15/2004

logography of ppR$_K$ (*14*). These observations probably correlate with the high thermal stability of ppR$_K$, as ppR$_K$ is stable even at 170 K, while the L intermediate appears in BR at this temperature (*7*). Accompanying the relaxation of ppR$_K$, the M intermediate of *p*pR (ppR$_M$) appears via deprotonation of the Schiff base. We previously reported that the C=O stretching vibrations of the protonated carboxyl group at 1765 cm^{-1} originated from Asp75 and that the N-like protein structure in *p*pR was not observed at alkaline pH (*15*). These observations suggested that the proton transfer mechanism in *p*pR is similar to that in BR, but the protein structural changes are different between them.

In the last step of the photocycle of *p*pR, the O intermediate (ppR$_O$) appears. In contrast to ppR$_K$ and ppR$_M$, our knowledge on ppR$_O$ remains limited. The reason is that ppR$_O$ is normally observed in the mixture with other intermediates such as ppR$_M$, and it is difficult to extract information on pure ppR$_O$. The previous time-resolved FTIR studies of *p*pR reported many important structural changes involving ppR$_O$ (*16*, *17*). However, it was not clear whether the observed vibrational bands indeed originate from ppR$_O$.

In this paper we attempted to obtain the ppR$_O$ minus *p*pR difference FTIR spectra. Since ppR$_M$ was also produced under the present experimental conditions (260 K and pH 5), we subtract the contribution of ppR$_M$ on the basis of UV−vis spectroscopy. The ppR$_O$ minus *p*pR difference spectra thus obtained are analyzed in detail. By use of the *p*pR samples with 12,14-D_2-labeled retinal, we determined the retinal configuration in ppR$_O$ to be all-trans. In ppR$_O$, C=O stretching vibrations of protonated carboxylates newly appear at 1757 (+)/1722 (−) cm^{-1} in H_2O and at 1747 (+)/1718 (−) cm^{-1} in D_2O in addition to the 1765 (+) cm^{-1} band of Asp75. Unique amide I vibrations are observed for ppR$_O$ that probe peptide backbone alterations. In addition, measurements upon hydration with D_2O or $D_2{}^{18}O$ revealed structural changes of water molecules in ppR$_M$ and ppR$_O$. Unlike the O intermediate of BR, ppR$_O$ is detected at 260 K, so that water vibrations can be examined. As a consequence, low-temperature FTIR measurements provided information on the water structural changes not only for ppR$_M$ but also for ppR$_O$. These observations are discussed in comparison with those of BR.

MATERIALS AND METHODS

Preparation of the ppR Samples. The *p*pR samples were prepared as described previously (*7*, *18*). Briefly, the *p*pR protein with a histidine tag at the C-terminus was expressed in *Escherichia coli*, solubilized with 1.5% *n*-dodecyl β-D-maltoside (DM), and purified by a Ni column. The purified *p*pR sample was then reconstituted into L-α-phosphatidylcholine (PC) liposomes by the removal of the detergent with Bio-Beads, where the molar ratio of the added PC to *p*pR was 50:1. The *p*pR samples with 12,14-D_2-labeled retinal were produced by adding 1 μM 12,14-D_2-labeled all-*trans*-retinal into the *E. coli* culture instead of the unlabeled all-*trans*-retinal.

FTIR Spectroscopy. FTIR spectroscopy was performed as described previously (*7*, *8*, *15*). The samples of *p*pR in PC liposomes were washed twice by buffers at pH 5.0 (2 mM citrate), pH 7.0 (2 mM phosphate), or pH 9.0 (2 mM borate). Ninety microliters of the *p*pR sample was dried on a BaF_2 window with a diameter of 18 mm. After hydration with H_2O, D_2O, or $D_2{}^{18}O$, the sample was placed in a cell, which was mounted in an Oxford DN-1704 cryostat placed in the Bio-Rad FTS-40 spectrometer. All spectra were measured with 2 cm^{-1} resolution. The ppR$_K$ minus *p*pR difference spectra were measured as follows (*7*). Illumination of the *p*pR film at pH 7 with 450 nm light at 77 K for 2 min converted *p*pR to ppR$_K$, and subsequent illumination with >560 nm light reverted ppR$_K$ to *p*pR. The difference spectrum was calculated from spectra constructed with 128 interferograms collected before and after the illumination. Twenty-four spectra obtained in this way were averaged for the ppR$_K$ minus *p*pR spectra.

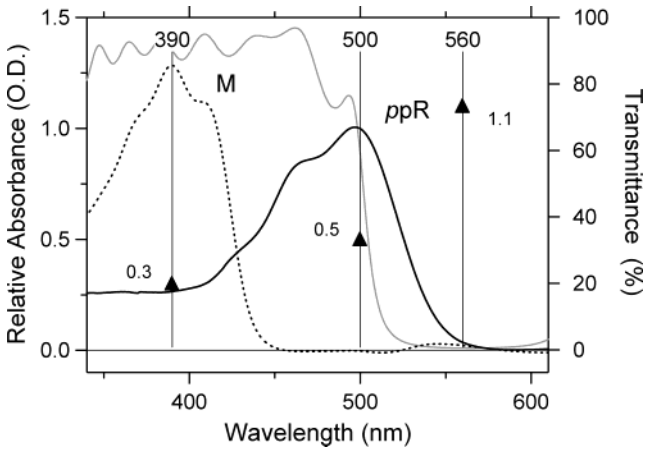

FIGURE 1: UV−vis absorption spectra of *p*pR and ppR$_M$ and transmittance spectrum of the optical filter used to accumulate ppR$_O$. The solid line and the dotted line represent the *p*pR and ppR$_M$ spectra, respectively. The solid gray line represents the transmittance spectrum of the optical filter for accumulation of ppR$_O$. The filled triangles denote relative absorbance of ppR$_O$ at 390, 500, and 560 nm, derived from Miyazaki et al. (*19*).

The ppR$_M$ minus *p*pR difference spectra were measured at 250 K and pH 9 as follows (*15*). To convert *p*pR to ppR$_M$, the sample was irradiated for 90 s with >480 nm light; subsequent illumination with UV light reverted ppR$_M$ to *p*pR. The difference spectrum was calculated from the spectra constructed with 64 interferograms collected after and before the illumination. Twenty-four spectra obtained in this way were averaged for the ppR$_M$ minus *p*pR spectra.

The ppR$_O$ minus *p*pR difference spectra were measured at 260 K and pH 5. To accumulate ppR$_O$ efficiently, the sample was irradiated for 2 min with the light through the band path filter whose transmittance spectrum was shown as a gray line in Figure 1. After being in the dark for 2 min, ppR$_O$ reverted to *p*pR almost completely (as shown in the text). The difference spectrum was calculated from the spectra constructed with 32 interferograms collected after and before the illumination and before and after relaxing in the dark. It should be noted that the data acquisition time after illumination is between 4.5 and 30 s under the present conditions. Sixteen spectra obtained in this way were averaged.

The obtained difference spectrum, however, contained ppR$_M$ in the product, so that we had to subtract the ppR$_M$ minus *p*pR spectrum to obtain the ppR$_O$ minus *p*pR spectrum. The amount of the residual ppR$_M$ in the difference spectrum at 260 K was estimated by means of kinetic UV−vis measurements as follows.

UV−Vis Measurements. Hydrated films were used as for the FTIR spectroscopy. After hydration by either H_2O or D_2O, the sample was placed in a cell, which was mounted in an Oxford DN-1704 cryostat placed in the JASCO V-550 spectrometer.

The UV−vis spectrum of *p*pR at pH 5 was measured at 260 K. The UV−vis spectrum of *p*pR$_M$ at pH 9 was measured at 240 K, not at 250 K, because some amounts of *p*pR$_M$ reverted to the original state during the UV−vis measurement at 250 K. The residual *p*pR component after illumination with >480 nm light was subtracted using the *p*pR spectrum taken at 240 K, and the resulting spectrum of *p*pR$_M$ was as shown in Figure 1. The *p*pR$_O$ spectrum could not be obtained because the *p*pR$_O$ intermediate reverted to the original state during the UV−vis measurement. Then, we assumed the relative absorbance of *p*pR$_O$ to be 0.30 at 390 nm, 0.50 at 500 nm, and 1.10 at 560 nm according to Miyazaki et al. (*19*). As a consequence, the time-dependent absorbance changes at each wavelength are described as follows.

$$\text{abs (390 nm)} = 0.27 \times p\text{pR} + 1.28 \times p\text{pR}_M + 0.30 \times p\text{pR}_O$$

$$\text{abs (500 nm)} = 1.00 \times p\text{pR} + 0.50 \times p\text{pR}_O$$

$$\text{abs (560 nm)} = 0.06 \times p\text{pR} + 1.10 \times p\text{pR}_O$$

From these equations, the time-dependent relative concentration changes can be calculated as follows.

$$p\text{pR}_M = 0.78 \times \text{abs (390 nm)} - 0.20 \times \text{abs (500 nm)} - 0.12 \times \text{abs (560 nm)}$$

$$p\text{pR}_O = 0.94 \times \text{abs (560 nm)} - 0.056 \times \text{abs (500 nm)}$$

$$p\text{pR} = 1.03 \times \text{abs (500 nm)} - 0.47 \times \text{abs (560 nm)}$$

We determined the amounts of *p*pR$_O$ and *p*pR$_M$ during the FTIR measurements according to these equations on the basis of time-resolved UV−vis measurement data between 4.5 and 30 s (shaded regions in Figure 2).

Time-dependent absorbance changes at 390, 500, and 560 nm at 260 K were measured as follows. After reaching a photo-steady state by illumination with light through the band-pass filter (whose transmittance spectrum is shown as a gray line in Figure 1) for 2 min, the absorbance changes were measured with 1 s intervals at each wavelength (Figure 2a,b). Each absorbance change shown is an average of three measurements.

RESULTS

The ppR$_O$ minus ppR Spectra Determined by UV−Vis Measurements. Dotted lines in Figure 3 show the IR difference spectra at 260 K and pH 5. The shift of the ethylenic C=C stretching vibrations to lower frequency (from 1550 to 1538 cm^{-1}) clearly shows the appearance of the red-shifted intermediate, presumably *p*pR$_O$. However, these spectra also contain the contribution of *p*pR$_M$, so that it is necessary to subtract the *p*pR$_M$ minus *p*pR difference spectra to obtain the pure *p*pR$_O$ minus *p*pR difference spectra. Since

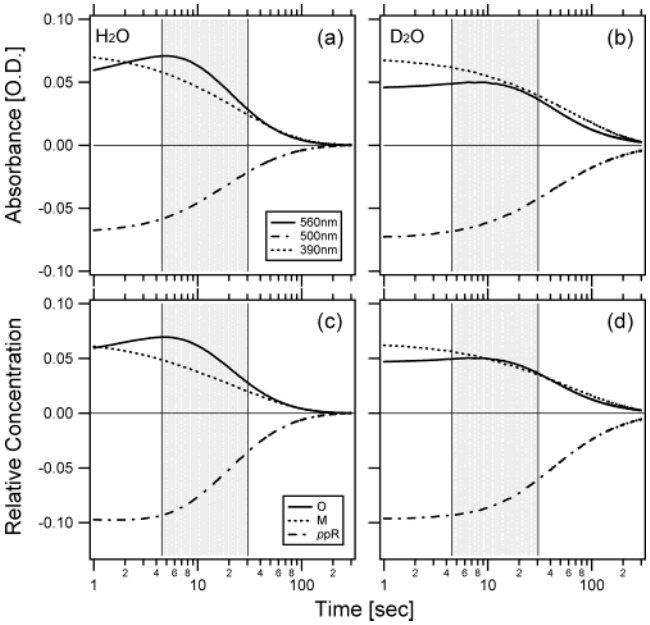

FIGURE 2: UV−vis absorbance changes at 390, 500, and 560 nm and relative concentration changes of *p*pR, *p*pR$_M$, and *p*pR$_O$ after the relaxation of the photoequilibrium mixture produced by illumination through the optical filter whose transmittance spectrum is shown in Figure 1. The measurements were done with H_2O (a) and D_2O (b). The relative concentration changes in H_2O (c) and D_2O (d) are calculated by the method described in the Materials and Methods section. FT-IR spectra were collected during the times represented by shaded regions (from 4.5 to 30 s).

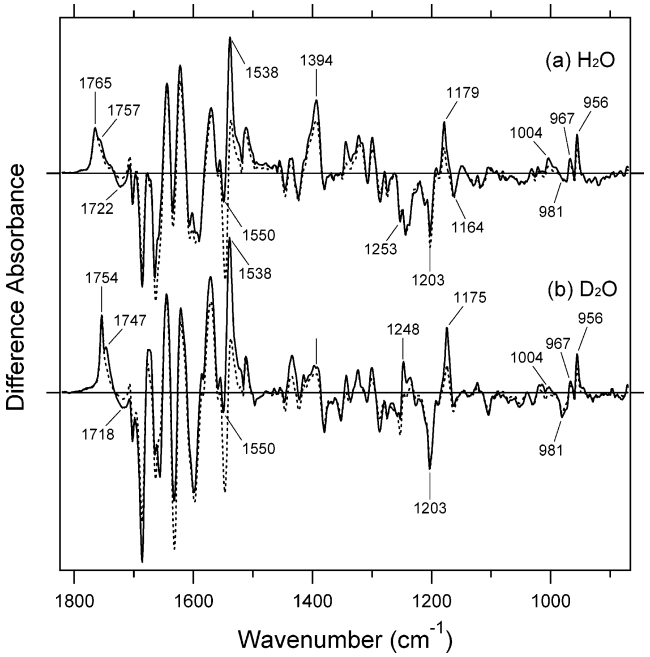

FIGURE 3: *p*pR$_O$ minus *p*pR infrared difference spectra in the 1820−870 cm^{-1} region. The solid lines are pure *p*pR$_O$ minus *p*pR spectra which are made by subtracting the *p*pR$_M$ component from the raw spectra drawn in dotted lines. These spectra were measured at 260 K and pH 5 upon hydration with H_2O (a) and D_2O (b). One division of the *y*-axis corresponds to 0.01 absorbance unit.

we know the shape of the *p*pR$_M$ minus *p*pR difference spectra (*15*), we can calculate the *p*pR$_O$ minus *p*pR difference spectra if we obtain the ratio of *p*pR$_M$ to *p*pR$_O$ in the product. In this case, the *p*pR$_M$-specific band is normally used as a marker for proper subtraction of the *p*pR$_M$ minus *p*pR spectra. It is, however, known that the *p*pR$_M$ minus *p*pR spectra do

not exhibit many positive bands (*15*, *20*). One of the characteristic bands is the positive 1765 cm^{-1} band due to protonated Asp75 (*15*), but the dotted lines in Figure 3a suggest that *p*pR_O also possesses the positive band at the same frequency. Thus, we determine the ratio of *p*pR_M and *p*pR_O during the FTIR measurements by kinetic UV−vis measurements.

Panels a and b of Figure 2 show the absorbance changes at 390, 500, and 560 nm during the relaxation of the photoequilibria at 260 K and pH 5 upon hydration with H_2O and D_2O, respectively. Absorbance changes at 390, 500, and 560 nm mainly originate from *p*pR_M, *p*pR, and *p*pR_O, respectively (Figure 1). By use of absorbance of each state at three wavelengths, we are able to calculate the ratio of *p*pR_M to *p*pR_O during the FTIR measurements (4.5−30 s; shaded regions in Figure 2). According to the equations in the Materials and Methods section, we determined the kinetic traces of *p*pR, *p*pR_M, and *p*pR_O in panel c (in H_2O) and panel d (in D_2O) of Figure 2. The obtained ratios of *p*pR_M to *p*pR_O during the FTIR measurements are 39:61 in H_2O (Figure 2c) and 49:51 in D_2O (Figure 2d).

The present UV−vis measurements showed that about half of the product in the raw spectra at 260 K and pH 5 (dotted lines in Figure 3) is *p*pR_M. If we add the three kinetic traces in Figure 2c,d, their sum will be zero for both H_2O and D_2O. This fact indicates that the relative absorbances of *p*pR_M, *p*pR, and *p*pR_O in Figure 1 are reasonable. This also suggests that other spectral species such as the N intermediate can be excluded from the present analysis. In contrast, the same kinetics at room temperature [such as in Miyazaki et al. (*19*)] are highly different from those in Figure 2, as the decay of *p*pR_M coincides with the appearance of *p*pR_O in the former. In the present study, both *p*pR_M and *p*pR_O seem to be equilibrated and decay in parallel (Figure 2). Such difference presumably originates from use of different temperatures (room temperature vs 260 K). It is likely that at 260 K *p*pR_O can be trapped (unlike the O intermediate of BR) but not as a pure state (like the O intermediate of BR).

The ppR$_O$ minus ppR Difference Spectra in the 1820−870 cm^{-1} Region. The solid lines in Figure 3 show the pure *p*pR_O minus *p*pR difference spectra calculated by subtracting the *p*pR_M minus *p*pR spectra from the raw spectra (Figure 3, dotted lines) according to the ratio determined by the UV−vis measurements. The ethylenic stretching vibrations at 1538 and 1550 cm^{-1} clearly show that the obtained spectra are the difference spectra between *p*pR_O and *p*pR. The 1164, 1203, and 1253 cm^{-1} bands are the C−C stretching vibrations of retinal in *p*pR and were already described in the literature (*7*). The positive bands at 1179 cm^{-1} in H_2O and at 1175 cm^{-1} in D_2O show that the retinal Schiff base of *p*pR_O is protonated and these bands derived from the C−C stretching vibrations near the Schiff base because of the deuterium effect (4 cm^{-1}). Similar bands were observed in the N intermediate of BR at 1185 cm^{-1} (*21*, *22*) and in the O intermediate of BR at 1168 cm^{-1} (*22*, *23*). The N and O intermediates of BR have different retinal configurations. The former has a 13-*cis*-retinal, while the latter has an all-*trans*-retinal. Therefore, these frequencies have been regarded as markers of the 13-cis or all-trans chromophore. The observed frequencies at 1179 cm^{-1} in H_2O and at 1175 cm^{-1} in D_2O are located in between, so that we cannot conclusively identify the retinal configuration of *p*pR_O without using labeled retinals.

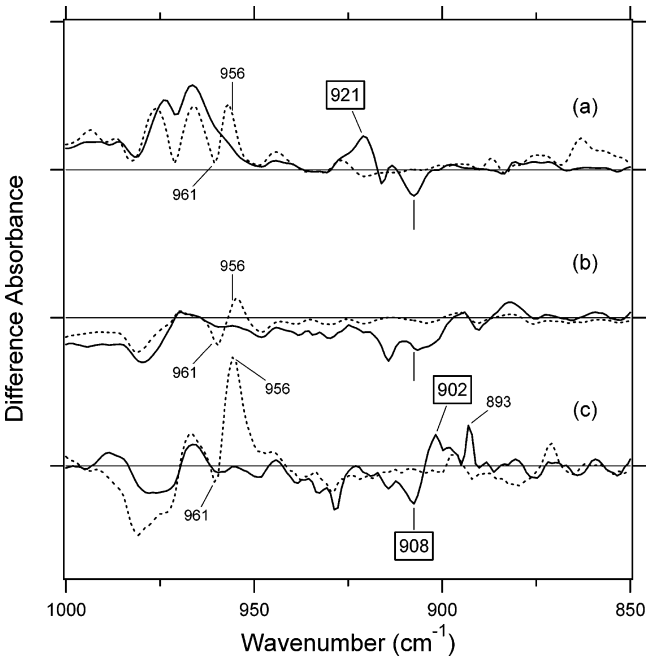

FIGURE 4: Bands from $C_{12}D + C_{14}D$ rocking vibrations in the *p*pR_K minus *p*pR (a), the *p*pR_M minus *p*pR (b), and the *p*pR_O minus *p*pR (c) spectra. The solid lines were obtained from the *p*pR sample reconstituted with 12,14-D_2-retinal. In the 935−890 cm^{-1} region, there are no bands in the native *p*pR sample reconstituted with unlabeled retinal as shown by the dotted lines. These spectra were measured at 77 K and pH 7 (a), 250 K and pH 9 (b), and 260 K and pH 5 (c) upon hydration with D_2O. One division of the *y*-axis corresponds to 0.0024 absorbance unit.

In the HOOP region, deuterium-insensitive bands at 956 and 967 cm^{-1} and a deuterium-sensitive band at 1004 cm^{-1} appear at the positive side. These positive bands suggest that the retinal chromophore of *p*pR_O is twisted similar to that in the O intermediate of BR (*23*). The *p*pR samples reconstituted with the 12,14-D_2-labeled retinal lack the 956 cm^{-1} band in the *p*pR_O minus *p*pR spectra (Figure 4c), indicating that the HOOP vibration at 956 cm^{-1} originates from C_{12}-H and/or C_{14}-H. In the *p*pR_K minus *p*pR difference infrared spectra, there are four positive bands and one negative band in addition to these bands. The deuterium-sensitive positive bands at 994, 987, and 979 cm^{-1} and the deuterium-insensitive bands at 1023 (+) and 1013 (−) cm^{-1} appear in the *p*pR_K minus *p*pR spectra (*7*). The appearance of fewer HOOP bands in the *p*pR_O minus *p*pR spectra suggests that the chromophore of *p*pR_O is less distorted than that of *p*pR_K.

Determination of the Retinal Configuration in the Intermediates of ppR. The retinal configuration, either all-trans or 13-cis, can be determined by use of 12,14-D_2-retinal (*24*). Curry et al. demonstrated that the frequencies of the in-phase rocking vibrations of the C_{12} and C_{14} hydrogens are sensitive to the configuration about the C_{13}═C_{14} bond (*24*). When the C_{12} and C_{14} positions are deuterated, the dependence of these frequencies on the C_{13}═C_{14} configuration is most apparent, because their rocking vibrations are shifted into the 1050−900-cm^{-1} range, where they are relatively isolated from C−C stretches and other CCH rocks. In fact, in-plane rocking vibrations of $C_{12}D + C_{14}D$ appear at 901 and 936 cm^{-1} for all-*trans*- and 13-*cis*-retinal, respectively, in solution (*24*). Smith et al. demonstrated that the bands are located at 914

cm^{-1} for BR and the O intermediate of BR that have all-*trans*-retinal but at 941 cm^{-1} for the dark-adapted bacteriorhodopsin that has 13-*cis*-retinal (*23*). Thus, the difference in frequency of about 30 cm^{-1} for 12,14-D_2-retinal can be a good indicator of isomeric state.

We measured the *p*pR_K minus *p*pR, *p*pR_M minus *p*pR, and *p*pR_O minus *p*pR difference spectra of the *p*pR sample reconstituted with the 12,14-D_2-retinal (Figure 4). In the 935−890 cm^{-1} region, there are no bands for the native *p*pR sample reconstituted with unlabeled retinal (dotted lines). In contrast, clear bands were observed for all of the spectra with the labeled retinal. The *p*pR_K minus *p*pR spectrum exhibits positive and negative bands at 921 and 908 cm^{-1}, respectively (Figure 4a), which can be interpreted in terms of 13-*cis*- and all-*trans*-retinal, respectively. The *p*pR_M minus *p*pR spectrum exhibits only negative bands (Figure 4b), presumably because of the reduction of the positive signal intensity due to the retinal Schiff base deprotonation in *p*pR_M. The negative band at 908 cm^{-1} corresponds to the in-phase rocking vibration of the $C_{12}D + C_{14}D$ combination in *p*pR. The *p*pR_O minus *p*pR spectrum exhibits positive and negative bands at 902 and 908 cm^{-1}, respectively (Figure 4c), and no positive bands in the 940−920 cm^{-1} region. From such a low frequency (902 cm^{-1}), we concluded that *p*pR_O possesses all-*trans*-retinal as is the case for the O intermediate of BR.

It is noted that the previous studies by use of 12,14-D_2-retinal were performed by resonance Raman spectroscopy (*23*, *24*), and in-phase rocking vibrations are weaker in IR measurements. In such case, downshifts of HOOP vibrations at positions C_{12}-H and/or C_{14}-H have to be taken into account, because they could appear in the 935−890 cm^{-1} region. Figure 4 shows that the *p*pR_K minus *p*pR, *p*pR_M minus *p*pR, and *p*pR_O minus *p*pR difference spectra all possess positive and negative bands at 956 and 961 cm^{-1}, respectively (dotted lines), that disappear in the 12,14-D_2-labeled sample (solid lines), whereas other HOOP bands are insensitive to the 12,14-D_2 label. Interestingly, corresponding bands in the lower frequency side are not clear for the 12,14-D_2-labeled sample, suggesting that the origin of the 961 (−)/956 (+) cm^{-1} bands may not be common. A sharp positive band at 893 cm^{-1} in the *p*pR_O minus *p*pR difference spectrum of the 12,14-D_2-labeled sample may correspond to that at 956 cm^{-1} (Figure 4c). Importantly, the positive band at 956 cm^{-1} is only HOOP band sensitive to the 12,14-D_2 label in the *p*pR_O minus *p*pR difference spectrum, while two positive peaks appear at 902 and 893 cm^{-1} for the 12,14-D_2-labeled sample. This suggests that one of them does not originate from the HOOP band. In addition, there are no positive bands in the 940−920 cm^{-1} region that corresponds to the in-phase rocking vibration of the 13-cis form in the *p*pR_O minus *p*pR difference spectrum (Figure 4c), being in contrast to the *p*pR_K minus *p*pR difference spectrum (Figure 4a). These observations support the present assignment as the in-phase rocking vibrations, and we concluded that the chromophore of *p*pR_O is all-trans form.

Spectral Comparison of the ppR_K minus ppR, ppR_M minus ppR, and ppR_O minus ppR Difference Spectra in the 1820−1580 cm^{-1} Region. The infrared difference spectra in this frequency region mainly monitor protein structural changes. In our previous papers, we showed that the carbonyl stretching vibrations of Asn105 appear at 1704 (−)/1699 (+) cm^{-1} (*25*) and at 1707 (+)/1701 (−) cm^{-1} (*15*) in the *p*pR_K minus *p*pR (Figure 5a) and *p*pR_M minus *p*pR (Figure 5b) difference spectra, respectively. We also assigned the protonated carboxyl stretching vibrations of Asp75 at 1764 cm^{-1} in H_2O and at 1753 cm^{-1} in D_2O (Figure 5b) (*15*). Figure 5c shows that the bands of Asn105 and Asp75 remain at 1707 (+)/1701 (−) cm^{-1} and 1765 cm^{-1} upon the *p*pR_O formation, respectively, while positive and negative bands newly appear at 1757 and 1722 cm^{-1}, respectively, in H_2O. These bands are downshifted to 1747 and 1718 cm^{-1} in D_2O. Therefore, these bands probably originate from protonated carboxylic acids. The positive band at 1757 cm^{-1} in H_2O and at 1747 cm^{-1} in D_2O is also observed by time-resolved FTIR measurements by Hein et al. (*16*) and Bergo et al. (*17*). In contrast, Hein et al. did not report on the negative 1722 cm^{-1} band in H_2O (the 1718 cm^{-1} band in D_2O), possibly because of the presence of other states in the mixture. On the other hand, Bergo et al. observed the negative band at 1724 cm^{-1} in H_2O and at 1719 cm^{-1} in D_2O also, but the bands were narrower.

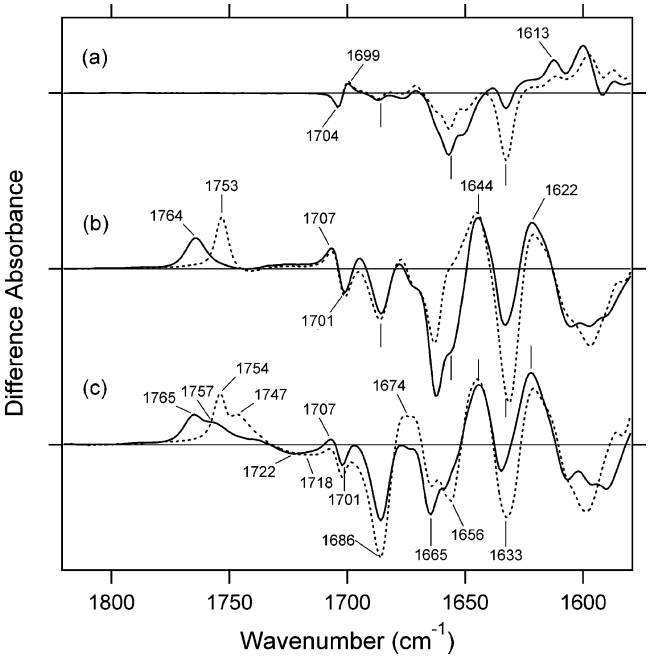

FIGURE 5: The *p*pR_K minus *p*pR (a), the *p*pR_M minus *p*pR (b), and the *p*pR_O minus *p*pR (c) spectra measured in the 1820−1580 cm^{-1} region, mostly characteristic for protein vibrations. The samples were hydrated with either H_2O (solid lines) or D_2O (dotted lines). These spectra were measured at 77 K and pH 7 (a), 250 K and pH 9 (b), and 260 K and pH 5 (c). One division of the *y*-axis corresponds to 0.012 absorbance unit.

In the 1690−1610 cm^{-1} region containing the amide I vibration, the features of the *p*pR_O minus *p*pR spectrum (Figure 5c) are similar to those of the *p*pR_M minus *p*pR spectrum (Figure 5b) but different from those of the *p*pR_K minus *p*pR spectrum (Figure 5a). The negative 1656 cm^{-1} bands in H_2O are assigned to the C=N stretching vibrations of *p*pR, which are downshifted to 1633 cm^{-1} upon the hydration with D_2O (*9*). The bands at 1686 (−), 1665 (−), 1644 (+), 1633 (−), and 1622 (+) cm^{-1} are common to the *p*pR_M minus *p*pR and the *p*pR_O minus *p*pR spectra. It is, however, noted that the negative 1656 cm^{-1} band newly appears for the *p*pR_O minus *p*pR spectrum in D_2O (Figure 5c), suggesting that structural perturbations take place in the

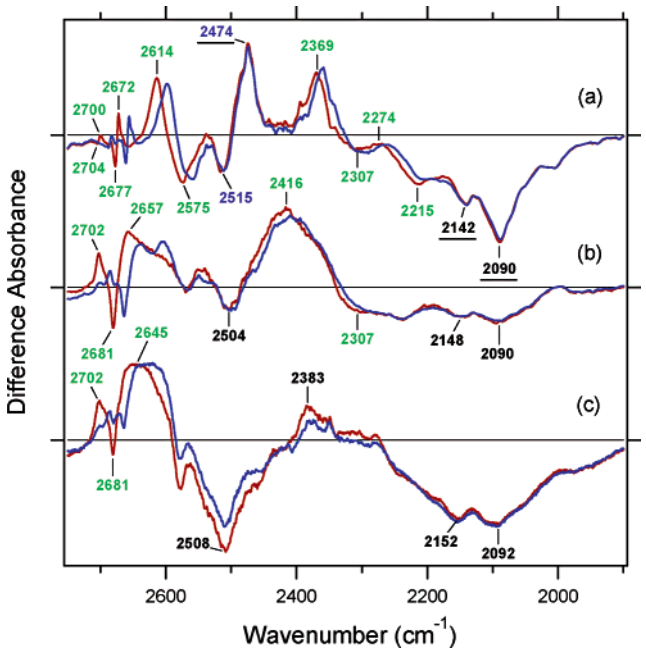

FIGURE 6: Comparison of the difference IR spectra of the samples hydrated with D_2O (red lines) or $D_2{}^{18}O$ (blue lines) in the 2750−1900 cm^{-1} region. The *p*pR_K minus *p*pR (a), the *p*pR_M minus *p*pR (b), and the *p*pR_O minus *p*pR (c) spectra were measured at 77 K and pH 7, 250 K and pH 9, and 260 K and pH 5, respectively. One division of the *y*-axis corresponds to 0.0015 absorbance unit. The frequencies labeled in green correspond to those identified as water stretching vibrations. The frequencies labeled in purple are O−D stretches of Thr79, while the underlined frequencies are N−D stretches of the Schiff base (*9*).

α-helix upon formation of *p*pR_O. In addition, the 1686 (−)/1674 (+) cm^{-1} bands in D_2O (Figure 5c) are characteristic for the *p*pR_O minus *p*pR spectrum and are assignable to amide I vibrations of turn structures.

Spectral Comparison of the ppR$_K$ minus ppR, ppR$_M$ minus ppR, and ppR$_O$ minus ppR Difference Spectra in the 2750−1900 cm^{-1} Region. Figure 6 shows a spectral comparison of the samples hydrated with D_2O (red lines) and $D_2{}^{18}O$ (blue lines) for *p*pR_K (a), *p*pR_M (b), and *p*pR_O (c). In the *p*pR_K minus *p*pR difference spectra, 10 peaks were assigned to O−D stretching vibrations of water molecules, where frequencies are widely distributed over the range of possible stretching vibrations of water (Figure 6a) (*8*). The hydrogen bond of the water O−D stretch at <2400 cm^{-1} is stronger than that of a fully hydrated tetrahedral water, suggesting that the O−D group interacts with a negative charge (*26*, *27*). Thus, the O−D stretches at 2307 and 2215 cm^{-1} are likely to belong to the water molecules which hydrate groups with negative charges in *p*pR. Higher frequency shifts upon *p*pR_K formation suggest that hydrogen bonds with negative charges are weakened upon photoisomerization. Similar observations were reported for BR, but with different frequencies (*27*).

In the *p*pR_M minus *p*pR difference spectra, five peaks exhibit the isotope-induced spectral downshift by 10−17 cm^{-1}, which are assigned to O−D stretching vibrations of water molecules (Figure 6b). The peaks at 2369 (+)/2307 (−) cm^{-1} in the *p*pR_K minus *p*pR difference spectra at 77 K remain at 2416 (+)/2307 (−) cm^{-1} in the *p*pR_M minus *p*pR difference spectra at 250 K, while the peaks at 2274 (+)/2215 (−) cm^{-1} disappear. The latter fact indicates that the hydrogen bond of the water molecule with the O−D stretch at 2215 cm^{-1} in *p*pR, the most strongly hydrogen-bonded water, possesses the same strength as that in *p*pR_M. A similar observation was made for BR, where the corresponding 2171 cm^{-1} band, which has been identified as the O−D stretch of a bridging water molecule hydrating Asp85 (*28*), is also restored in its M intermediate (*29*).

In the *p*pR_O minus *p*pR difference spectra, three peaks at 2702 (+), 2681 (−), and 2645 (+) cm^{-1} were assigned as O−D stretches of water on the basis of the isotope shift (Figure 6c). There are no peaks at <2400 cm^{-1}, indicating that the strongly hydrogen-bonded water molecules whose O−D stretches are at 2307 and 2215 cm^{-1} are present both in *p*pR and in *p*pR_O. The baseline variates considerably around 2500 cm^{-1} (absolute absorption maximum of X−D stretch) at 260 K, which also influences the spectral comparison in Figure 6c. Nevertheless, no isotope shifts were observed at <2600 cm^{-1}.

Thus, vibrational analysis of strongly hydrogen-bonded water molecules can be summarized as follows. Two water O−D stretches at 2307 and 2215 cm^{-1} in *p*pR are weakened upon formation of *p*pR_K (Figure 6a). In *p*pR_M, the 2215 cm^{-1} band is restored by forming a strong hydrogen bond again, whereas the weakened O−D stretch of the 2307 cm^{-1} band is further weakened as shown by the spectral upshift to 2416 cm^{-1} (Figure 6b). This change is also restored in *p*pR_O by forming a strong hydrogen bond again (Figure 6c). As a consequence, the strongly hydrogen-bonded water molecules apparently exhibit no changes of their hydrogen bonds, even though Asp75 is protonated.

On the higher frequency side of the *p*pR_M minus *p*pR difference spectra, three peaks are assigned as water O−D stretches at 2702 (+), 2681 (−), and 2657 (+) cm^{-1} (Figure 6b). These water molecules possess weak hydrogen bonds, and the spectra are similar to those of BR (*29*). The corresponding O−H stretches are at 3654 (+), 3629 (−), and 3588 (+) cm^{-1} (data not shown). This is similar to the *p*pR_O minus *p*pR difference spectra, which possess positive 2702 cm^{-1} and negative 2681 cm^{-1} bands (Figure 6c). On the other hand, the difference spectra slightly differ at 2650−2600 cm^{-1}. Strong water bands at 2614 (+)/2575 (−) cm^{-1} in the *p*pR_K minus *p*pR were not observed for the late photointermediates.

Besides the water O−D stretches, the *p*pR_K minus *p*pR difference spectra exhibit the vibrational bands at 2515 (−), 2474 (+), 2142 (−), and 2090 (−) cm^{-1} (Figure 6a). Previously, we found that the peaks at 2515 and 2474 cm^{-1} originate from the O−D stretch of Thr79, while the peaks at 2474, 2142, and 2090 cm^{-1} were assigned to the N−D stretch of the protonated retinal Schiff base (*9*). Similar negative peaks are also observed at 2504, 2148, and 2090 cm^{-1} in the *p*pR_M minus *p*pR spectra or at 2508, 2152, and 2092 cm^{-1} in the *p*pR_O minus *p*pR spectra. Assignment of the corresponding positive peaks requires isotope labeling and/or mutants. Nevertheless, the presence of the negative peaks at 2152 and 2092 cm^{-1} in the *p*pR_O minus *p*pR spectra suggests that the hydrogen bonds of the protonated retinal Schiff base are considerably weakened upon *p*pR_O formation, the positive band at 2383 cm^{-1} being a candidate for the upshifted N−D stretch (Figure 6c).

DISCUSSION

In this paper, we studied *p*pR$_O$ by means of FTIR and UV−vis spectroscopy. By use of UV−vis spectroscopy, we determined the ratio of *p*pR$_M$ to *p*pR$_O$ during the FTIR measurements. Consequently, we obtained the *p*pR$_O$ minus *p*pR infrared difference spectra in H_2O and D_2O (solid lines in Figure 3). In addition, we determined the retinal configuration of *p*pR$_O$ to be all-trans by use of the *p*pR sample reconstituted with 12,14-D_2 isotope-labeled retinal. We also assigned the O−D stretches of water molecules in *p*pR$_O$ as well as *p*pR$_M$ for the first time.

The Chromophore Structure in ppR$_O$. Hein et al. previously argued that the configuration of retinal in *p*pR$_O$ is all-trans from the similarity of the C−C stretching vibrations of retinal to those in BR (*16*). In this study, we identified the retinal configuration in *p*pR$_O$ as all-trans, because the in-phase rocking vibrations of $C_{12}D + C_{14}D$ combination (902 cm^{-1}) are very similar to those of all-*trans*-retinal in solution (901 cm^{-1}) (Figure 4c) (*24*). The 12,14-D_2-labeled samples also show the disappearance of the 956 cm^{-1} band in the *p*pR$_O$ minus *p*pR spectra, indicating that the HOOP vibration at 956 cm^{-1} originates from C_{12}-H and/or C_{14}-H. The all-trans chromophore of *p*pR$_O$ seems to be twisted in the middle.

The hydrogen bond of the retinal Schiff base is also important. Although the hydrogen-bonding strength has been examined through the C=N stretching vibrations (through the difference between positions of C=NH and C=ND), Figure 5c does not clearly show the C=N stretches of *p*pR$_O$ at the positive side. On the other hand, the N−D stretch of the Schiff base in D_2O is a more direct marker of the hydrogen-bonding strength of the Schiff base, where the frequency is lower when a hydrogen bond is stronger (*30*−*32*). Figure 6c shows the presence of the bands at 2152 and 2092 cm^{-1}, which presumably originate from the N−D stretch of the Schiff base. Since there are no bands at their lower frequency side, the N−D stretch of *p*pR$_O$ is located at higher frequency. This indicates that the hydrogen bond of the Schiff base is not restored in *p*pR$_O$, being considerably weaker than in *p*pR. In *p*pR, a hydrogen-bonding acceptor of the Schiff base is a water molecule (water 402) (*10*, *11*). This fact may suggest that this water molecule does not return to the original position in *p*pR$_O$. Another possibility is that the N−H (N−D) group points differently because of a twist in the chromophore, even when the water returns to the original position. We infer that the former is more likely because Asp75 is still protonated in *p*pR$_O$ and the water-containing hydrogen-bonding network is not restored. Further discussion is presented as follows.

Protonated Carboxylates in ppR$_O$. Time-resolved FTIR measurements that probe *p*pR$_M$ and *p*pR$_O$ were reported by Hein et al. (*16*) and Bergo et al. (*17*). Although they could not obtain the pure *p*pR$_O$ minus *p*pR spectra, they observed the C=O stretching vibrations of protonated carboxylates in the 1780−1710 cm^{-1} region. Hein et al. argued that the newly appeared 1757 cm^{-1} band in H_2O originated from protonation of Asp201 in *p*pR$_O$ (*16*). On the other hand, Bergo et al. argued that the 1757 cm^{-1} band is downshifted from 1764 cm^{-1} upon the *p*pR$_O$ formation, indicating that the 1757 cm^{-1} band originates from the protonated Asp75 (*17*). Bergo et al. also showed that the negative 1724 cm^{-1} band appears at pH 6, but not upon complex formation with *p*HtrII. They suggested that the 1724 cm^{-1} band originates from Asp193, whose pK_a value was reported to be about 6 in the presence of chlorine (*33*). They assumed that the presence of *p*HtrII decreases the pK_a value of Asp193.

The present *p*pR$_O$ minus *p*pR spectra clearly show the presence of positive bands at both 1765 and 1757 cm^{-1} (Figure 5c), excluding the possibility that the 1757 cm^{-1} band originates from Asp75. In fact, the 1765 cm^{-1} band never lacks the intensity in the M-to-O transition. Thus, the newly appeared bands at 1757 and 1722 cm^{-1} probably originate from other carboxylic groups, such as Asp193 or Asp201. In this case, chloride ion may play important roles, because Asp193 is located near the chloride binding site (*11*). The assignment of the 1757 and 1722 cm^{-1} bands is in progress.

Protein Structure in ppR$_O$. The pure *p*pR$_O$ minus *p*pR difference spectra now allow a spectral comparison in the amide I vibrational region that monitors peptide backbone alteration. Panels a and b of Figure 5 clearly show that the peptide backbone is more altered in *p*pR$_M$ than in *p*pR$_K$, as evidenced by the greater spectral changes. In contrast, many vibrational bands are common for *p*pR$_M$ and *p*pR$_O$. The negative 1665 cm^{-1} band corresponding to distorted α-helix is observed for both *p*pR$_M$ and *p*pR$_O$. In contrast, the negative 1656 cm^{-1} band that corresponds to a typical α-helix newly appears for the *p*pR$_O$ minus *p*pR spectrum in D_2O (Figure 5c). Thus, the M-to-O transition is accompanied by structural perturbation of α-helices.

Another noteworthy issue is the 1686 (−)/1674 (+) cm^{-1} bands in D_2O (Figure 5c) characteristic of the *p*pR$_O$ minus *p*pR spectrum. Bergo et al. observed the 1686 cm^{-1} band in the *p*pR−*p*HtrII fusion complex also (*17*). They reported that this band was prominent in the presence of *p*HtrII and thus probes the structural changes induced by the transducer. However, the present study showed that the *p*pR$_O$ minus *p*pR difference spectra possess an intense negative band at 1686 cm^{-1} even in the absence of *p*HtrII. In fact, this negative band has the largest amplitude in the 1600−1800 cm^{-1} region both in H_2O (solid line in Figure 5c) and in D_2O (dotted line in Figure 5c). The apparent increase of the amplitude of this negative band in the presence of transducer reported in Bergo et al. (*16*) might originate from an equilibrium shift from *p*pR$_M$ to *p*pR$_O$. Since we obtained the pure *p*pR$_O$ minus *p*pR difference spectra in this study, similar measurements in the presence of transducer are interesting and will be our future focus.

Internal Water Molecules in ppR$_M$ and ppR$_O$. Internal water molecules play important roles in archaeal rhodopsins, and low-temperature FTIR spectroscopy is a powerful tool to investigate water structural changes during their functional processes (*26*). Earlier, we published the *p*pR$_K$ minus *p*pR difference spectra in the entire water stretching vibrational region (Figure 6a) (*8*), where five water O−D stretching vibrations are widely distributed over the possible stretching vibrations of water for both *p*pR$_K$ and *p*pR. It should be noted that the hydrogen bonding of water molecules with O−D stretches at $<$2400 cm^{-1} is stronger than that of a fully hydrated tetrahedral water. Thus, we concluded that the O−D stretches at 2307 and 2215 cm^{-1} correspond to internal water molecules hydrating negative charges in *p*pR. The Schiff base region of *p*pR contains three water molecules that constitute roughly planar pentagonal cluster, whose structure is similar to that in BR. In the case of BR, similar bands were observed

at 2323, 2292, and 2171 cm^{-1} (*27*, *29*), and the lowest frequency band (2171 cm^{-1}) was recently assigned to the O−D stretch of water 402 (the bridging water between the Schiff base and Asp85) hydrogen-bonded with Asp85 (*28*). Our conclusion is also consistent with the quantum chemical and molecular dynamics calculations (*34*). Although the locations of water bands are not identified for *p*pR, it would be a reasonable postulation that the lowest frequency band (2215 cm^{-1}) is the bridging water between the Schiff base and Asp75.

Formation of *p*R_M is accompanied by the proton transfer from the Schiff base to Asp75. In general, the Schiff base deprotonation reaction is a crucial step in the function of rhodopsins. For instance, it triggers sequential proton transfer reactions for the light-driven proton pump BR, and the M formation also correlates with the switch reaction to determine the vectoriality (*35*, *36*). In addition, deprotonation of the Schiff base leads to an activated form in the light-signal conversions of archaeal and visual rhodopsins. In *p*pR and BR, the proton donor and acceptor are rather close to each other [4.0 Å for *p*pR (*10*) and 4.4 Å for BR (*12*)], and a mechanism of proton transfer between them has been a point of interest. In the case of BR, we found that the lowest frequency water band at 2171 cm^{-1} is restored in the M intermediate even though Asp85 has no negative charge (*29*). Since only Asp212 possesses a negative charge in the Schiff base region, we interpreted that the water molecule hydrates Asp212 in the M intermediate. In other words, switch of a strong hydrogen bond of a water from Asp85 to Asp212 contributes to the proton transfer reaction from the Schiff base to Asp85; we thus called this mechanism the "hydration switch model".

In the case of *p*pR, we still have to assign the water bands. Nevertheless, as described above, the frequency at 2215 cm^{-1} is low enough to be considered as belonging to the bridging water molecule similar to water 402 in BR (2171 cm^{-1}). As in BR, the *p*pR_M minus *p*pR difference spectra lack the negative band at 2215 cm^{-1} (Figure 6b), indicating that the water finds the hydrogen-bonding acceptor in *p*pR_M. Taking in account that the hydrogen-bonding acceptor is negatively charged, it should be Asp201 in *p*pR_M that corresponds to Asp212 in BR. Thus, the hydration switch model developed for BR can also be applied to *p*pR for the proton transfer mechanism from the Schiff base to Asp75. Spectral features of the higher frequency side (2700−2600 cm^{-1}) are also similar between *p*pR and BR (*29*). One of the interesting differences between *p*pR and BR lies in the other bands. In BR, the difference spectra lack not only the 2171 cm^{-1} band but also the bands at 2323 and 2292 cm^{-1} (*29*). In contrast, the negative water band at 2307 cm^{-1} is preserved in the *p*pR_M minus *p*pR difference spectra (Figure 6b). This fact suggests that the hydrogen-bonding network in the M states of *p*pR is rearranged differently from that of BR, though the same mechanism drives the proton transfer reaction.

Water structural changes in the last step of the photocycle, namely, in the O intermediate, are also interesting. However, in the case of BR, the O intermediate cannot be trapped at low temperatures, so that we have not studied water O−D stretching vibrations of the O intermediate so far. The advantage of the *p*pR study is that *p*pR_O can be trapped at 260 K, so that we are able to study water stretching vibrations in *p*pR_O. In this study, we could indeed obtain the information on water bands of the O intermediate for the first time. In the *p*pR_O minus *p*pR difference spectra, the O−D stretches of water appeared only in the >2600 cm^{-1} region (Figure 6c). The difference spectra lack the water bands at 2307 and 2215 cm^{-1}, suggesting that the hydration structures of internal water molecules are considerably restored in *p*pR_O. It should be, however, noted that *p*pR_O possesses protonated Asp75 like *p*pR_M. This may suggest that Asp201 is not protonated in *p*pR_O, since it is the only negative charge in the Schiff base region. The hydrogen-bonding acceptor of the water at 2307 cm^{-1} is also of interest, and the future mutation studies will lead to a better understanding of water structural changes during the photocycle of *p*pR.

ACKNOWLEDGMENT

We thank K. Kamada, M. Sumii, and Y. Sudo for valuable discussion.

REFERENCES

1. Kamo, N., Shimono, K., Iwamoto, M., and Sudo, Y. (2001) Photochemistry and Photoinduced Proton-Transfer by *Pharaonis* Phoborhodopsin, *Biochemistry (Moscow) 66*, 1277−1282.
2. Sasaki, J., and Spudich, J. L. (2000) Proton transport by sensory rhodopsins and its modulation by transducer-binding, *Biochim. Biophys. Acta 1460*, 230−239.
3. Spudich, J. L., and Lanyi, J. K. (1996) Shuttling between two protein conformations: the common mechanism for sensory transduction and ion transport, *Curr. Opin. Cell Biol. 8*, 452−457.
4. Furutani, Y., and Kandori, H. (2002) Internal water molecules of archaeal rhodopsins, *Mol. Membr. Biol. 19*, 257−265.
5. Kandori, H., Tomioka, H., and Sasabe, H. (2002) Excited-State Dynamics of *pharaonis* Phoborhodopsin Probed by Femtosecond Fluorescence Spectroscopy, *J. Phys. Chem. A 106*, 2091−2095.
6. Lutz, I., Sieg, A., Wegener, A. A., Engelhard, M., Boche, I., Otsuka, M., Oesterhelt, D., Wachtveitl, J., and Zinth, W. (2001) Primary reactions of sensory rhodopsins, *Proc. Natl. Acad. Sci. U.S.A. 98*, 962−967.
7. Kandori, H., Shimono, K., Sudo, Y., Iwamoto, M., Shichida, Y., and Kamo, N. (2001) Structural changes of *pharaonis* phoborhodopsin upon photoisomerization of the retinal chromophore: infrared spectral comparison with bacteriorhodopsin, *Biochemistry 40*, 9238−9246.
8. Kandori, H., Furutani, Y., Shimono, K., Shichida, Y., and Kamo, N. (2001) Internal Water Molecules of *pharaonis* Phoborhodopsin Studied by Low- Temperature Infrared Spectroscopy, *Biochemistry 40*, 15693−15698.
9. Shimono, K., Furutani, Y., Kamo, N., and Kandori, H. (2003) Vibrational Modes of the Protonated Schiff Base in *pharaonis* Phoborhodopsin, *Biochemistry 42*, 7801−7806.
10. Luecke, H., Schobert, B., Lanyi, J. K., Spudich, E. N., and Spudich, J. L. (2001) Crystal Structure of Sensory Rhodopsin II at 2.4 A: Insights into Color Tuning and Transducer Interaction, *Science 293*, 1499−1503.
11. Royant, A., Nollert, P., Edman, K., Neutze, R., Landau, E. M., Pebay-Peyroula, E., and Navarro, J. (2001) X-ray structure of sensory rhodopsin II at 2.1-Å resolution, *Proc. Natl. Acad. Sci. U.S.A. 98*, 10131−10136.
12. Luecke, H., Schobert, B., Richter, H. T., Cartailler, J. P., and Lanyi, J. K. (1999) Structure of bacteriorhodopsin at 1.55 Å resolution, *J. Mol. Biol. 291*, 899−911.
13. Belrhali, H., Nollert, P., Royant, A., Menzel, C., Rosenbusch, J. P., Landau, E. M., and Pebay-Peyroula, E. (1999) Protein, lipid and water organization in bacteriorhodopsin crystals: a molecular view of the purple membrane at 1.9 Å resolution, *Struct. Folding Des. 7*, 909−917.
14. Edman, K., Royant, A., Nollert, P., Maxwell, C. A., Pebay-Peyroula, E., Navarro, J., Neutze, R., and Landau, E. M. (2002) Early structural rearrangements in the photocycle of an integral membrane sensory receptor, *Structure 10*, 473−482.
15. Furutani, Y., Iwamoto, M., Shimono, K., Kamo, N., and Kandori, H. (2002) FTIR Spectroscopy of the M Photointermediate in *pharaonis* Phoborhodopsin, *Biophys. J. 83*, 3482−3489.

16. Hein, M., Wegener, A. A., Engelhard, M., and Siebert, F. (2003) Time-Resolved FTIR Studies of Sensory Rhodopsin II (NpSRII) from *Natronobacterium pharaonis*: Implications for Proton Transport and Receptor Activation, *Biophys. J. 84*, 1208−1217.
17. Bergo, V., Spudich, E. N., Spudich, J. L., and Rothschild, K. J. (2003) Conformational changes detected in a sensory rhodopsin II-transducer complex, *J. Biol. Chem. 278*, 36556−36562.
18. Shimono, K., Ikeura, Y., Sudo, Y., Iwamoto, M., and Kamo, N. (2001) Environment around the chromophore in *pharaonis* phoborhodopsin: mutation analysis of the retinal binding site, *Biochim. Biophys. Acta 1515*, 92−100.
19. Miyazaki, M., Hirayama, J., Hayakawa, M., and Kamo, N. (1992) Flash photolysis study on *pharaonis* phoborhodopsin from a haloalkaliphilic bacterium (*Natronobacterium pharonis*), *Biochim. Biophys. Acta 1140*, 22−29.
20. Engelhard, M., Scharf, B., and Siebert, F. (1996) Protonation changes during the photocycle of sensory rhodopsin II from *Natronobacterium pharaonis*, *FEBS Lett. 395*, 195−198.
21. Maeda, A. (1995) Application of FTIR spectroscopy to the structural study on the function of bacteriorhodopsin, *Isr. J. Chem. 35*, 387−400.
22. Zscherp, C., and Heberle, J. (1997) Infrared difference spectra of the intermediates L, M, N, and O of the bacteriorhodopsin photoreaction obtained by time-resolved attenuated total reflection spectroscopy, *J. Phys. Chem. B 101*, 10542−10547.
23. Smith, S. O., Pardoen, J. A., Mulder, P. P. J., Curry, B., Lugtenburg, J., and Mathies, R. A. (1983) Chromophore structure in bacteriorhodopsin's O640 photointermediate, *Biochemistry 22*, 6141−6148.
24. Curry, B., Palings, I., Broeck, A., Pardoen, J. A., Lugtenburg, J., and Mathies, R. A. (1984) Vibrational analysisof 13-cis-retinal, *J. Phys. Chem. 88*, 688−702.
25. Kandori, H., Shimono, K., Shichida, Y., and Kamo, N. (2002) Interaction of Asn105 with the retinal chromophore during photoisomerization of pharaonis phoborhodopsin, *Biochemistry 41*, 4554−4559.
26. Kandori, H. (2000) Role of internal water molecules in bacteriorhodopsin, *Biochim. Biophys. Acta 1460*, 177−191.
27. Kandori, H., and Shichida, Y. (2000) Direct Observation of the Bridged Water Stretching Vibrations Inside a Protein, *J. Am. Chem. Soc. 122*, 11745−11746.
28. Shibata, M., Tanimoto, T., and Kandori, H. (2003) Water molecules in the schiff base region of bacteriorhodopsin, *J. Am. Chem. Soc. 125*, 13312−13313.
29. Tanimoto, T., Furutani, Y., and Kandori, H. (2003) Structural changes of water in the schiff base region of bacteriorhodopsin: proposal of a hydration switch model, *Biochemistry 42*, 2300−2306.
30. Aton, B., Doukas, A. G., Narva, D., Callender, R. H., Dinur, U., and Honig, B. (1980) Resonance Raman studies of the primary photochemical event in visual pigments, *Biophys. J. 29*, 79−94.
31. Gilson, H. S., Honig, B. H., Croteau, A., Zarrilli, G., and Nakanishi, K. (1988) Analysis of the factors that influence the C═N stretching frequency of polyene Schiff bases. Implications for bacteriorhodopsin and rhodopsin, *Biophys. J. 53*, 261−269.
32. Baasov, T., Friedman, N., and Sheves, M. (1987) Factors affecting the C═N stretching in protonated retinal Schiff base: a model study for bacteriorhodopsin and visual pigments, *Biochemistry 26*, 3210−3217.
33. Iwamoto, M., Kandori, H., and Kamo, N. (2003) Photochemical properties of *pharaonis* phoborhodopsin (Sensory rhodopsin II), *Recent Res. Dev. Chem. 1*, 15−30.
34. Hayashi, S., and Ohmine, I. (2000) Proton transfer in bacteriorhodopsin: structure, excitation, IR spectra, and potential energy surface analyses by an ab initio QM/MM Method, *J. Phys. Chem. B 104*, 10678−10691.
35. Lanyi, J. K. (2000) Molecular Mechanism of Ion Transport in Bacteriorhodopsin: Insights from Crystallographic, Spectroscopic, Kinetic, and Mutational Studies, *J. Phys. Chem. B 104*, 11441−11448.
36. Haupts, U., Tittor, J., and Oesterhelt, D. (1999) Closing in on bacteriorhodopsin: progress in understanding the molecule, *Annu. Rev. Biophys. Biomol. Struct. 28*, 367−399.

BI036316B